

Measured wavenumber: Frequency spectrum associated with acoustic and aerodynamic wall pressure fluctuations

Blandine Arguillat and Denis Ricot

Research Department Acoustics Group, TCR AVA 1 63, 1 Avenue du Golf, 78288 Guyancourt, France

Christophe Bailly^{a)} and Gilles Robert

Laboratoire de Mécanique des Fluides et d'Acoustique, Ecole Centrale de Lyon, UMR CNRS 5509, 36 Avenue Guy de Collongue, 69134 Ecully Cedex, France

(Received 16 December 2009; revised 15 July 2010; accepted 17 July 2010)

Direct measurements of the wavenumber-frequency spectrum of wall pressure fluctuations beneath a turbulent plane channel flow have been performed in an anechoic wind tunnel. A rotative array has been designed that allows the measurement of a complete map, 63×63 measuring points, of cross-power spectral densities over a large area. An original post-processing has been developed to separate the acoustic and the aerodynamic exciting loadings by transforming space-frequency data into wavenumber-frequency spectra. The acoustic part has also been estimated from a simple Corcos-like model including the contribution of a diffuse sound field. The measured acoustic contribution to the surface pressure fluctuations is 5% of the measured aerodynamic surface pressure fluctuations for a velocity and boundary layer thickness relevant for automotive interior noise applications. This shows that for aerodynamically induced car interior noise, both contributions to the surface pressure fluctuations on car windows have to be taken into account.

© 2010 Acoustical Society of America. [DOI: 10.1121/1.3478780]

PACS number(s): 43.28.Ra [AH]

Pages: 1647–1655

I. INTRODUCTION

Noise induced by wall pressure fluctuations is regularly encountered in engineering problems including flow noise in sonar domes for underwater applications, aircraft interior noise or space launchers among many others.^{1–3} The motivation of the present study is to better understand and predict noise transmitted to the interior of a passenger vehicle compartment.⁴ Comfort or use of high quality audio and vocal recognition systems require to reduce automobile aerodynamic noise. This so-called wind noise is found to be perceptible from 100 km h^{-1} , and becomes dominant for speeds greater than 130 km h^{-1} . Even for such low speed turbulent boundary layers, it seems that both aerodynamic and acoustic contributions have to be taken into account in the wall pressure field excitation.^{5,6} The acoustic component is however smaller and difficult to discriminate.

The classical form of the wavenumber—frequency spectrum of the fluctuating wall pressure, say $\Phi(k_x, k_y, \omega)$, is shown in Fig. 1 in the (k_x, k_y) plane at a given frequency. The spectral density is dominated by the convective region centered on $k_x \simeq k_c$ and $k_y \simeq 0$. Compressibility effects are represented by the acoustic region defined by the disk $k \leq k_0$, with a peak at the sonic region $k = k_0$. Note that the acoustic and the convected wavenumbers are such that $k_0 = M_c k_c$ with $M_c \simeq 0.1$ for automotive applications. Furthermore, the bending wavenumber $k_f \sim \sqrt{\omega}$ is also drawn with a dashed circle.

Transmission noise across a side glass consists of resonant and non-resonant radiating modes of the structure. By

considering a free bending wave propagating in a plate, critical frequencies associated with the aerodynamic loading $f_c = U_c^2 \sqrt{\rho_s / D} / (2\pi) = \mathcal{O}(10 \text{ Hz})$ and with the acoustic loading $f_c = c_0^2 \sqrt{\rho_s / D} / (2\pi) = \mathcal{O}(10^3 \text{ Hz})$ can be estimated. As shown in Fig. 1 for a low Mach number turbulent boundary layer, a significant contribution of the acoustic loading is expected in the high-frequency case (c), especially around the critical frequency, even if the acoustic excitation is not the most energetic part of the wall pressure spectrum.

Physical models based on simplified analytical approach⁷ or Statistical Energy Analysis⁵ indicate that the acoustic power radiated by a panel submitted to an acoustic field at a given level is 15 to 30 dB higher than the acoustic power radiated by the same panel excited by a turbulent field with the same level. In other words, the transmission efficiency of an acoustic field is about 15–30 dB higher than the transmission efficiency of an aerodynamic pressure field. The exact frequency-dependent transmission efficiency depends of course on the detailed parameters of the excitation pressure fields such as correlation lengths or characteristics wavelengths, and on the material properties of the glass. As a consequence, even if the acoustic wall pressure level induced by turbulent flow is generally much lower than the associated aerodynamic pressure, say 20 dB lower, the contribution of this field to the internal noise can be important, if not dominant.

A first approach for experimental investigations of wall pressure spectra in wavenumber space consists of a direct measurement of the cross-power spectral densities by spatial discrete Fourier transform. A low-pass wavenumber filtering and a great number of sensors are thus required. This is why very few and only recent studies using this method are avail-

^{a)}Author to whom correspondence should be addressed. Electronic mail: christophe.bailly@ec-lyon.fr

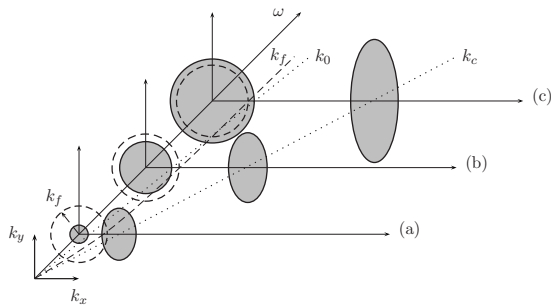


FIG. 1. Wall pressure spectrum of a low Mach number turbulent boundary layer in the (k_x, k_y) plane for a given frequency ω : (a) for $k_0 \leq k_f \sim k_c$, (b) for $k_0 < k_f < k_c$ and (c) for $k_f < k_0 < k_c$.

able; see Ibars,⁸ Manoha⁹ or Abraham.¹⁰ A second approach is based on the analysis of the vibratory response of a structure excited by the turbulent pressure fluctuations. Each vibration mode filters, at its own frequency, the wavenumbers associated to its modal shape. Robert¹¹ for instance used small rectangular vibrating plates whose responses are known, see also the review by Blake.¹ A main disadvantage of this technique lies in the fact that only a few wavenumbers are accessible. A third way is to use arrays of pressure transducers. Maidanik¹² describes the wavevector filtering action of transducer arrays. Maidanik and Jorgensen¹³ propose also enhancements to such arrays. The principle consists in obtaining, through linear combinations of signals, a wavenumber spectrum for discrete values of the wavenumber, depending on the spacing between transducers. Many authors^{8,9,14,15} put this method into practice. Assuming that longitudinal and transversal fluctuations are independent as suggested by Corcos,¹⁶ they only measured one-dimensional spectra in both directions.

In the present work, direct measurements of the two-dimensional wavenumber—frequency spectrum of a wall pressure field induced by a turbulent boundary layer are reported. Moreover, a post-processing is applied to separate acoustic and aerodynamic excitations. Few studies were conducted in two dimensions, and the work of Sherman *et al.*¹⁷ using a 11×11 transducers square array for a water boundary layer can be mentioned.

The paper is organized as follows. The experimental arrangement is described in Section II, and the signal processing used to evaluate spectrum-wavenumber spectra is given in Section III. This post-processing is applied to the case of a turbulent boundary layer in Section IV and concluding remarks are summarized in Section V.

II. EXPERIMENTAL PROCEDURE

A. Remote microphone probes

The considered application requires a high spatial resolution, a small background noise and a large frequency range. However traditional pressure transducers used in aerodynamic measurements present a high background noise, and the acoustic transducers are of too high sensitivity, typically piezoelectric transducers or condenser microphones of diameter 1-in. or $\frac{1}{2}$ -in. In term of sensitivity, $\frac{1}{4}$ -in. and $\frac{1}{8}$ -in. could have been suitable, but the first ones are too big-sized and

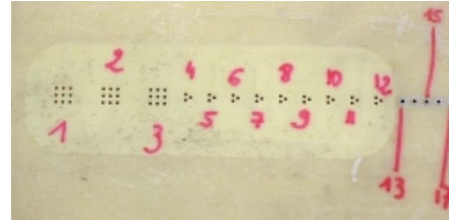
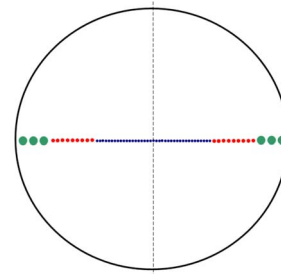


FIG. 2. (Color online) Sketch of the rotative measurement array, and picture showing the arrangement of the holes on the wall at one end.

the others are often too expensive. Non point sensors also induce a spatial averaging over their sensitive surface. This effect, initially studied by Corcos,¹⁶ has then been reformulated by Lueptow¹⁸ to take different types of transducers into account. One possible solution to reduce the size of the sensitive surface is to use pinhole microphones. Widely used, for example by Callister,¹⁹ Farabee and Casarella^{20,21} or Brungart *et al.*,²² this system does not yet permit to bring the transducers closer from each other.

The choice has thus been made to use remote microphone probes. The interest of such a setting is twofold: on the one hand the active measurement surface is reduced to the size of the tube at the wall, and on the other hand the viscous dissipation effects in the tube attenuate the level of pressure fluctuations. A classical acoustical microphone of high sensitivity can then be used. In the present work, each probe is composed of a $\frac{1}{4}$ -in. Brüel & Kjær Type-4935 microphone, placed perpendicularly to a steel tube of variable diameter, and of length from 14 to 15 cm. At one end, the tube comes out on the measurement wall. At the other end, each metallic tube is linked to a 2 m long, 2 mm diameter choked vinyl tube. In this way, reflexions inside the tubes can be avoided.

Three different kinds of probes have been designed. For the big diameter probes, the metallic tube diameter is 5 mm and an adapter is used to join the vinyl tube. For the medium diameter probes, the section is constant, with a 2 mm diameter tube. For the small diameter probes, the section of the tube progressively decreases to reach a diameter of 0.7 mm at the wall. Since a large hole on the wall could have induced disturbing whistling and non-negligible flow rate fluctuations, the tubes of big and medium diameter probes do not come out directly on the wall, but through little holes of diameter 0.5 mm, 9 holes for big diameter probes and 3 holes for the medium ones, as shown in Fig. 2.

The frequency response function has been characterized in amplitude and phase using a calibration tube. The calibration tube allows to generate an acoustic plane wave up to 13 kHz which is measured with a reference microphone

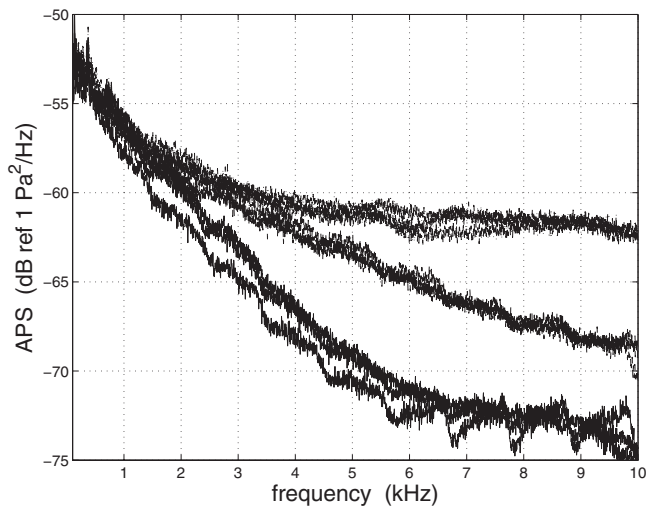


FIG. 3. Auto-power spectral (APS) densities of wall pressure fluctuations measured by the three kinds of probes under a turbulent boundary layer at $U_\infty=44 \text{ m s}^{-1}$ and $\text{Re}_{\delta^*} \approx 5.5 \times 10^4$. From bottom to top: — big probes, --- medium probes and small probes.

mounted near the open end of the tube. The open end of this tube is placed above each pinhole, or each group of holes for the medium and big diameter probes, and the transfer function is measured between the remote microphone and the reference microphone.²³ A similar procedure has been used by Leclercq and Bohineust.²⁴

B. Array

The measurement array is obtained by placing $N=63$ remote microphone probes along the diameter of a disk. Figure 2 shows the position of the transducers on this disk. On each side of the central transducer, 19 small-diameter probes are placed, with a spacing of $\Delta r_1=2 \text{ mm}$ between the center of two adjacent transducers. On both sides of small probes, there are 2×9 probes of diameter 2 mm, spaced by $\Delta r_2=4 \text{ mm}$. Lastly, 2×3 probes of 5 mm diameter are placed on both sides of medium-diameter probes, and are spaced by $\Delta r_3=8 \text{ mm}$.

The measurement consists of the simultaneous recording of the pressure field measured by the probes during the time $T_m=90 \text{ s}$. After recording the N pressure signals during T_m , the transducers line is turned by an angle of $\Delta\theta$ around the center and the process is then repeated $M=63$ times to scan the complete disk, with $\Delta\theta=\pi/M \approx 2.9^\circ$. In this way, a grid of $63 \times 63=3969$ measuring points is built up. All the data are collected with a 64-channel MKII Müller-BBM acquisition system.

Figure 3 shows the auto-power spectral densities of wall pressure fluctuations measured by the three kinds of probes under a turbulent boundary layer. Three beams of curves can be identified, each corresponding to a different kind of probe. As predicted by the theory,^{16,18} the biggest transducers have the lowest cut-off frequency, around 1500 Hz. The cut-off frequency of the medium-sized probes is about 3000 Hz. The small-diameter probes beam does not show any slope changing, which means that their cut-off frequency is above 10 kHz. Big and medium probes serve as low-pass wavenumber filters to eliminate large wavelengths and play a role of anti-

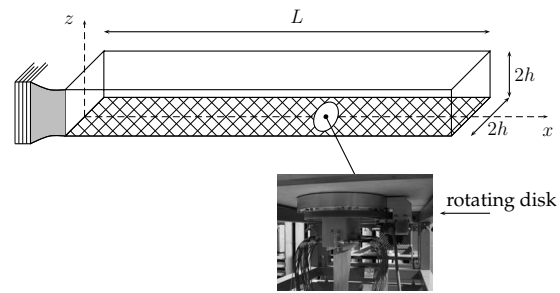


FIG. 4. Test channel mounted on the outlet of the wind tunnel. The square duct has a width of $2h=0.5 \text{ m}$ and a test-section length of a 4 m. The rotating array of remote microphones is located at $x=2.5 \text{ m}$.

aliasing filter. What should also be noted in Fig. 3 is that, except at high frequencies, each probes response has been calibrated well enough to eliminate the own probe oscillatory response such that level differences among the same kind of probes remain in an acceptable range of 2 dB. However, and by caution, data above 6000 Hz which have demonstrated to present calibration errors, will not be used in this study.

C. Experimental setup

The experiments were conducted in the main subsonic wind tunnel of the Centre Acoustique at Ecole Centrale de Lyon in France.^{25,26} The flow is generated by a 350 kW Neu centrifugal blower delivering a nominal mass flow rate of 15 kg s^{-1} , and the fan is powered by an electronically controlled Tridge-Electric LAK 4280A motor. Air passes through a settling chamber including a honeycomb and several wire meshes designed to reduce free stream turbulence. Acoustic treatment on the wind tunnel walls and baffled silencers allows to reduce the noise level and to prevent contamination of acoustic measurements performed in the anechoic chamber. This results in an air flow at ambient temperature with a low background noise and low residual turbulence intensity, less than 1%.

As shown in Fig. 4, the flow is finally accelerated in a convergent and then guided into a large anechoic room of $10 \times 8 \times 8 \text{ m}^3$, by a 4-m-long square duct with a cross section of $0.5 \times 0.5 \text{ m}^2$. The studied boundary layer develops naturally on the floor of this test channel, and the rotating disk is mounted at a distance $x=2.5 \text{ m}$ from the convergent. Results for three velocities have been investigated²³ and only the case $U_\infty=44 \text{ m s}^{-1}$ is considered hereafter. The Reynolds number based on the boundary layer thickness is $\text{Re}_{\delta^*} = U_\infty \delta^* / \nu = 5.5 \times 10^4$, and the shape factor is $H = \delta^* / \delta_\theta \approx 1.19$ with $\delta^* \approx 19 \times 10^{-3} \text{ m}$. The mean velocity profile and the rms velocity fluctuations are shown in Fig. 5. The turbulence intensity reaches $u' / U_\infty \approx 0.1$ inside the boundary layer. The friction velocity is found to be $u^* / U_\infty \approx 0.036$ by fitting the mean velocity profile with a logarithmic law, which yields a Reynolds number $\text{Re}_{\delta_\theta}^* = u^* \delta_\theta / \nu \approx 1716$ and a ratio $u' / u^* \approx 2.7$ for the rms fluctuations, in agreement with other studies.^{21,26}

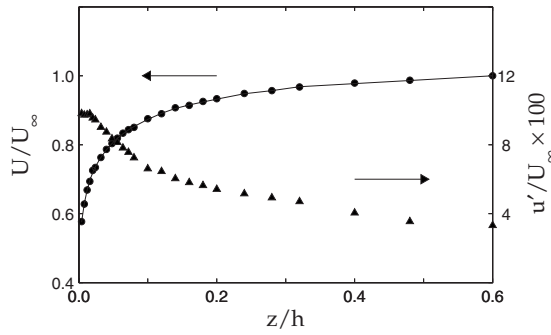


FIG. 5. Mean velocity profile (•) and turbulence intensity (▲) measured by hot wire anemometer in the boundary layer at $U_\infty=44$ m/s. The transverse distance z is normalized by the half-width h of the channel, refer to Fig. 4.

III. SIGNAL PROCESSING

The post-processing described in this section is the two-dimensional transformation of the spatial data into wavenumber spectra.

A. Computation of the wavenumber: Frequency spectrum

Let $p(\vec{r}, t)$ be a random stationary and ergodic signal depending on space and time. The finite Fourier transform in the time domain is defined by

$$P(\vec{r}, \omega) = \frac{1}{2\pi} \int_0^T p(\vec{r}, t) e^{i\omega t} dt, \quad (1)$$

where T is a time interval. The cross-power spectral density may be defined from the time Fourier transforms of the signals

$$S_{p_i p_j}(\vec{x}_i, \vec{r}, \omega) = \lim_{T \rightarrow \infty} \frac{2\pi}{T} E[P(\vec{x}_i, \omega) P^*(\vec{x}_j = \vec{x}_i + \vec{r}, \omega)], \quad (2)$$

where E stands for the mathematical expectation. Furthermore, the cross-power spectrum is only a function of the separation vector \vec{r} regardless of the observer point \vec{x}_i for a homogeneous field, that is $S_{p_i p_j}(\vec{x}_i, \vec{r}, \omega) = S_{p_i p_j}(\vec{r}, \omega)$. The cross-power spectral density as a function of frequency and wavenumber, commonly called wavenumber-frequency spectrum, is then defined as the spatial Fourier transform of $S_{p_i p_j}(\vec{r}, \omega)$

$$\Phi(\vec{k}, \omega) = \frac{1}{(2\pi)^2} \int \int_{-\infty}^{+\infty} S_{p_i p_j}(\vec{r}, \omega) e^{-i\vec{k} \cdot \vec{r}} d\vec{r}, \quad (3)$$

where the two-dimensional Fourier transform in the space domain is defined by

$$P(\vec{k}, t) = \frac{1}{(2\pi)^2} \int \int_{-\infty}^{+\infty} p(\vec{x}, t) e^{-i\vec{k} \cdot \vec{x}} d\vec{x}. \quad (4)$$

From Eq. (2), it is straightforward to show that the wavenumber-frequency spectral density is a real quantity for an homogeneous pressure field, i.e., $\Phi(\vec{k}, \omega) = \Phi^*(\vec{k}, \omega)$. Note also that the Parseval identity²⁷ is obtained by taking the inverse transform of Eq. (3), calculated at $\vec{r}=\vec{0}$

$$\int \int_{-\infty}^{+\infty} \Phi(\vec{k}, \omega) d\vec{k} = S_{p_i p_j}(\vec{r}=\vec{0}, \omega) = S_{pp}(\omega), \quad (5)$$

where S_{pp} is the frequency spectral density. In practice, the space integration in Eq. (3) is restricted to the rotating disk, and cross-spectral densities are measured at the points $\vec{x}_i = (r_n, \theta_m) = (n\Delta r, m\Delta\theta)$ using polar coordinates. The wavenumber-frequency spectrum Φ is thus estimated as follows:

$$\Phi(\vec{k}, \omega) = \frac{1}{(2\pi)^2} \sum_{m=1}^M \sum_{n=1}^N S_{p_n p_m}(r_n, \theta_m, \omega) \times e^{-i(r_n \cos \theta_m k_x + r_n \sin \theta_m k_y)} r_n \Delta r \Delta \theta. \quad (6)$$

The frequency cross-spectra (2) are calculated using the Welch periodogram method. The sampling frequency is 25.6 kHz and a Hanning windowing is applied to the time data blocks. Averaging is performed on 400 data blocks of 0.08 s with 50% overlapping. A simple rectangular windowing is kept for the space integration in Eq. (6) after preliminary tests on other windowings,²³ and the spectral step is $\Delta k = 6$ rad/m. Before studying the turbulent boundary layer case in Section IV, analytical verifications on the case of a diffuse sound field and on the Corcos turbulent boundary layer model are first presented in what follows to validate the implementation of the post-processing.

B. Validation on diffuse sound field

The frequency cross-power spectrum of a diffuse sound field is given by^{28,29}

$$S_{p_i p_j}(R, \Theta, \omega) = S_{pp}(\omega) \frac{\sin(k_0 R)}{k_0 R} \quad (7)$$

in spherical coordinates (R, Θ) . An analytical expression of the wavenumber-frequency spectrum (3) can then be expressed by taking the Fourier transform of the footprint. It yields

$$\Phi(\vec{k}, \omega) = \begin{cases} S_{pp}(\omega) \frac{1}{2\pi k_0^2 \sqrt{1 - (|\vec{k}|/k_0)^2}} & \text{if } |\vec{k}| < k_0 \\ 0 & \text{if } |\vec{k}| > k_0. \end{cases} \quad (8)$$

A pure tone diffuse sound field is considered in what follows, and the frequency cross-spectra (7) is projected on the array positions. The post-processing results are then compared with the analytical expression (8) in Fig. 6, and a good agreement is observed. However, three groups of wiggles, circles in the (k_x, k_y) plane, due to the aliasing induced by the spatial sampling of $\Phi(\vec{k}, \omega)$ are also visible. The smaller circles have a radius of $k_{\max 3} \pm k_0$ with $k_{\max 3} = 2\pi/\Delta r_3 \approx 393$ rad m^{-1} , and correspond to the aliasing induced by the most spaced transducers. The second group of circles correspond to $k_{\max 2} = 2\pi/\Delta r_2 \approx 785$ rad m^{-1} , and is induced by the medium-sized probes. The most important effect of spatial aliasing is visible at $k_{\max 1} = 2\pi/\Delta r_1 \approx 1570$ rad m^{-1} , due to spacing between the smallest probes. Note that another aliasing error generated by the discretization in the azimuthal direction can be also detected.²³

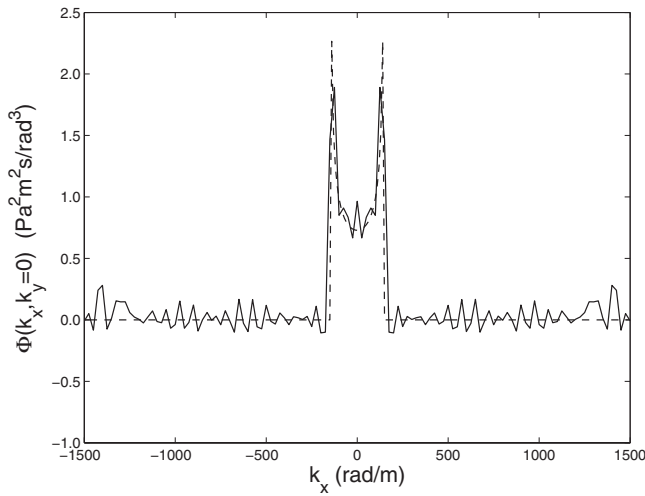


FIG. 6. Verification test case for a pure tone diffuse sound field, with $f_0 = 8$ kHz and $S_{pp} = 10^5$ Pa^2/Hz . Profile of $\Phi(\vec{k}, \omega_0)$ along the line $k_y = 0$, post-processing of the theoretical cross-power spectra in solid line, analytical expression given by Eq. (8) in dashed line.

C. Validation on the Corcos model

Corcos¹⁶ proposed a semi-empirical model for the spectral cross-power spectrum of wall pressure fluctuations beneath a turbulent boundary layer

$$S_{p_i p_j}(x, y, \omega) = A(\omega) e^{-(k_c/\alpha)|x|} e^{-(k_c/\beta)|y|} e^{ik_c x}, \quad (9)$$

where $k_c = \omega/U_c$ represents the convection of vortical structures at the velocity U_c . The corresponding wavenumber spectrum is then given by

$$\Phi(k_x, k_y, \omega) = \frac{A(\omega)}{\pi^2} \frac{\alpha k_c}{k_c^2 + \alpha^2(k_x - k_c)^2} \frac{\beta k_c}{k_c^2 + \beta^2 k_y^2} \quad (10)$$

As for the diffuse sound field, a comparison between the post-processing results and the analytical solution is shown in Fig. 7. The two spectra are very close, with a maximum at

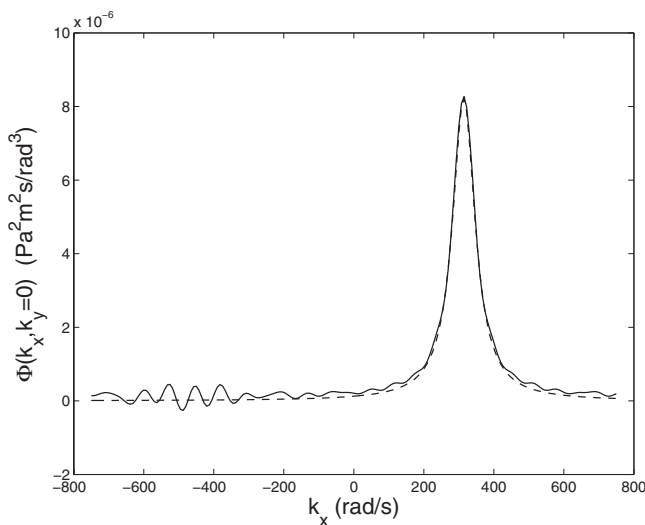


FIG. 7. Verification test case for the Corcos model, with $A=1$ Pa^2/Hz , $\alpha = 8$, $\beta=1$, $f=2$ kHz and $U_c=40$ m/s. Profile of $\Phi(\vec{k}, \omega_0)$ along the line $k_y = 0$. The convected wave number is $k_c = 100\pi$ rad m^{-1} . — post-processing of the theoretical cross-power spectra, - - - analytical expression given by Eq. (10).

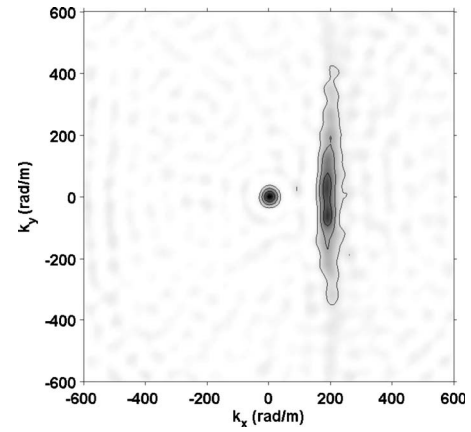


FIG. 8. Measured spectrum $\Phi(k_x, k_y, \omega)$ at $f=1000$ Hz in the wavenumber space induced by a turbulent boundary layer.

the convected wavenumber k_c and a peak width driven by the two coefficients α and β . Secondary lobes associated with the rectangular windowing are also visible.

IV. WAVENUMBER-FREQUENCY SPECTRUM OF A TURBULENT BOUNDARY LAYER

The post-processing presented in the previous section is now applied to measured data for the case of the turbulent boundary layer described in Section II C. The wavenumber-frequency spectra have been calculated on the pressure fluctuations recorded by the rotating array according to Eq. (6), and the spectrum for $f=1$ kHz is shown in Fig. 8 in the wavenumber space. Two contributions can be clearly identified in this plot. The aerodynamic spot can be recognized by its classical Corcos-like spectrum, and is located around $k_c \approx 188$ rad s^{-1} , which corresponds to a mean convection velocity of $U_c \approx 33$ m s^{-1} . In addition, a second spot corresponding to acoustic waves is also visible at low wavenumbers. The wavenumber resolution of the post-processing is not sufficient to accurately describe the directivity pattern, but no privileged direction of propagation seems noticeable, as expected for a diffuse sound field. In what follows, an evaluation of the acoustic part and the physical origin of this contribution are discussed.

The acoustic frequency spectrum can be first estimated by integrating $\Phi(\vec{k}, \omega)$ over the acoustic disk of radius $k_0 = \omega/c_0$, see expression (5). The evolution of $S_{pp}(\omega)$ for $k \leq k_0$ is shown in Fig. 9. Two peaks at about 345 and 690 Hz are clearly visible on the graph, and can be directly associated with modal resonances of the square-section duct. If we consider the wind tunnel duct as rigid, its resonance frequencies in the spanwise direction are given by $f_n = nc_0/2L$. With a transverse length $L=50$ cm, one gets $f_n \approx 343 \times n$ Hz, which closely corresponds to the measured peaks. Additional measurements have been conducted by submitting the test duct to a white noise and by recording the resulting pressure on the probes to support this interpretation.²³ First duct resonances are again found in the transfer function between the sound source and the probe array aligned along the longitudinal direction.

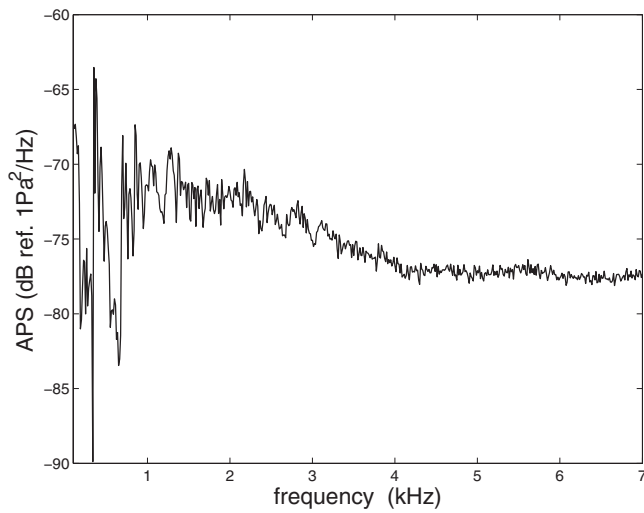


FIG. 9. Acoustical spectral density $S_{pp}(\omega)$ obtained by integration $\Phi(\vec{k}, \omega)$ over the acoustic disk $k \leq k_0$.

A second possible method to identify and characterize the acoustic component consists in studying the cross-power spectra $S_{p_i p_j}$. A coherence function γ is also introduced as follows

$$\gamma(r, \theta, \omega) = \frac{|S_{p_i p_j}|}{\sqrt{S_{p_i p_i} S_{p_j p_j}}} = \frac{|S_{pp}(r, \theta, \omega)|}{S_{pp}(0, 0, \omega)}. \quad (11)$$

An exponential shape is expected for γ according to Corcos's model, see Eq. (9) in previous section. In Fig. 10, $\ln(\gamma)$ is therefore plotted as a function of the distance r from the disk center. Regular oscillations around a mean value are found from experimental data, and can be attributed to the additional presence of an acoustic contribution to the aerodynamic part, which is generated by the turbulent boundary layer itself. A simple model of $S_{p_i p_j}$ can be proposed to explain this behavior. It is assumed that the wall pressure field is the sum of an aerodynamic contribution provided by Cor-

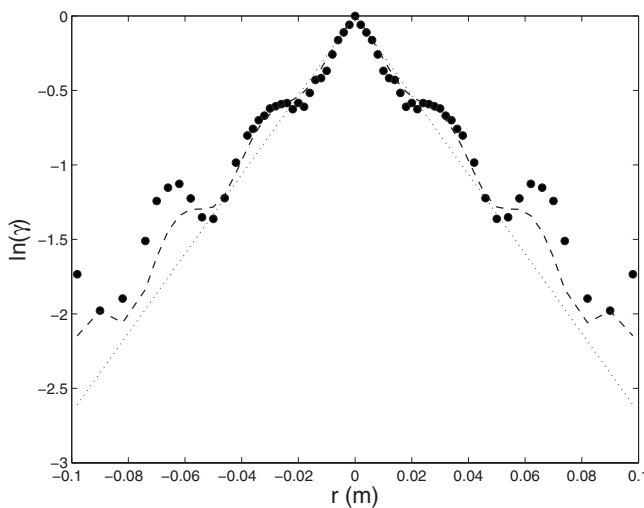
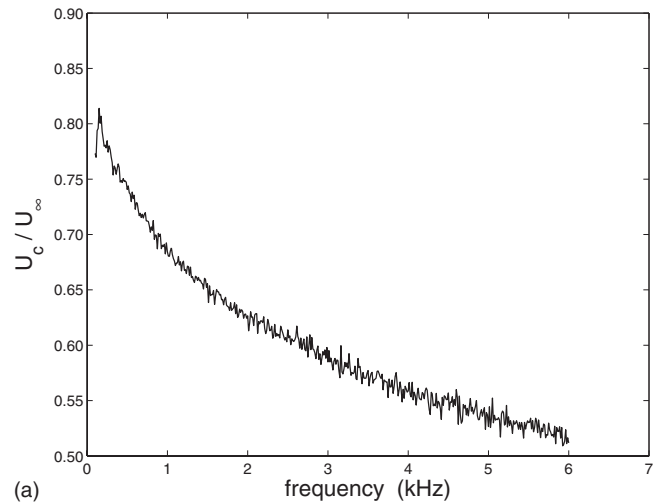
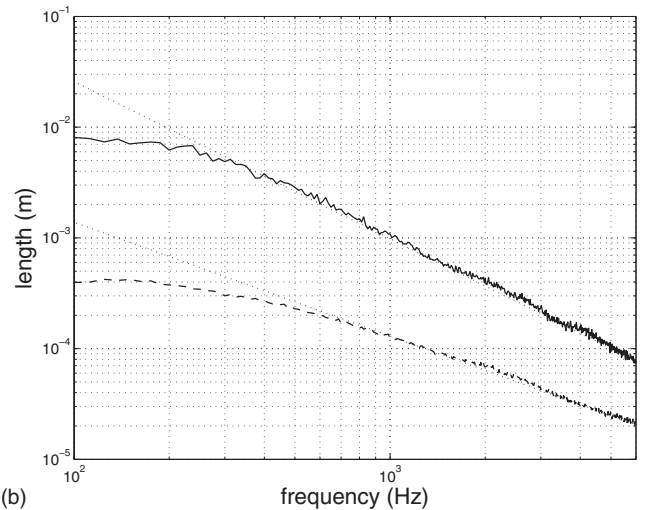


FIG. 10. Coherence function $\gamma(r)$, see Eq. (11), in the longitudinal direction at $f=1000$ Hz. ● experimental data, --- regression and linear regression.



(a)



(b)

FIG. 11. Computed parameters for the model (12). (a) Convection velocity U_c normalized by the free stream velocity U_c as a function of the frequency. (b) Longitudinal and transversal correlation lengths, $\alpha U_c / \omega$ in solid line and $\beta U_c / \omega$ in dashed line respectively.

cos's model and an acoustic part given by a diffuse sound field, in agreement with results reported in Fig. 8, so that

$$\frac{S_{pp}(r, \theta, \omega)}{S_{pp}(0, 0, \omega)} = \frac{1}{1+A} \left[e^{-\omega/(\alpha U_c)|r \cos \theta} e^{-\omega/(\beta U_c)|r \sin \theta} e^{i(\omega/U_c)r \cos \theta} + A \frac{\sin(k_0 r)}{k_0 r} \right] \quad (12)$$

The four parameters α , β , U_c and the acoustic magnitude A can be estimated from experimental points by a least mean square procedure. A similar idea was applied by Ibars,⁸ but a plane wave model was used to take account of the acoustic component. Only 11 regularly distributed angular position of the array have been used for determining these parameters. The convection velocity is shown in Fig. 11 (left). Decrease of the convection velocity while frequency increases has already been observed,¹ and is classically interpreted in term of size of structures. As frequency increases, the size of structures in the boundary layer, proportional to the wavelength, decreases. Small vortex are thus located nearer to the wall than large structures, and are sub-

mitted to a slower flow. Their convection velocity is therefore smaller. The longitudinal correlation length $\alpha U_c/\omega$ and the transversal correlation length $\beta U_c/\omega$ are also plotted in log-log as function of the frequency in Fig. 11 (right). The obtained curves tend to be linear in high frequency. Above 1000 Hz, the slope of the longitudinal correlation length curve is around -1 , and the slope of the transverse correlation length curve is around -1.4 . Therefore, even with a frequency-dependent convection velocity, both correlation lengths nearly evolve as the inverse of frequency which is in agreement with Corcos' assumption.¹⁶ In the low frequency range, correlation lengths tend to be constant. This behavior is in agreement with the findings of Cockburn and Robertson³⁰ or Efimtsov³¹ who proposed modification of Corcos' constant correlation coefficients to take account of the influence of finite boundary layer thickness, see also the review by Graham.³ Vortex size and thus correlation lengths are indeed limited by the boundary layer thickness. In frequency domain, it implies that correlation length cannot increase to infinite value as the frequency tends to zero.

It is worth noting that the analytical model (12) used for the aerodynamic part of the cross-power spectrum is not a Corcos model since physical parameters are allowed to vary as a function of frequency. This analytical model can be said to be a Corcos-like model. Other base models have been tested in this study. For instance, the same parametric estimation procedure has been apply using the Smol'yakov and Tkachenko³² model in Eq. (12). This model is not based on the lateral and longitudinal separation approach proposed by Corcos but it combines correlation lengths to generate a two-dimensional cross-spectrum with an ellipse pattern. Very similar results were obtained.

Finally, the acoustic magnitude represents about 5% of the aerodynamic magnitude for the main part of the frequency band, for $f \geq 1$ kHz, and at resonance frequencies of the duct, it reaches nearly 45% of the aerodynamical magnitude, demonstrating efficiency of resonance phenomena.

To report a more accurate comparison with the first calculation method, namely the direct integration of $\Phi(\vec{k}, \omega)$ over the acoustic disk, the acoustical magnitude has been multiplied by the measured auto-power spectrum $S_{pp}(\omega)$ to compute the absolute acoustic magnitude in Pa^2/Hz . Results obtained by both methods are shown in Fig. 12, and they are in very good agreement. The second resonance peak is not well marked with the integration method, probably because of a lack of accuracy due to the crude spectral sampling, $\Delta k = 6$ rad/s to compare with $k_0 = 18$ rad s^{-1} at 1 kHz for instance. Nevertheless, consistency between the two approaches is well verified.

Outside of the frequency ranges dominated by duct resonances, the difference between the acoustic component and the aerodynamic component is about 15 dB, see Fig. 12. It is much lower than the difference of 25 dB found in the simulations of Dejong *et al.*⁶ This latter value is based on an empirical estimation of the acoustic level using SEA computations of interior noise. The turbulent field is directly measured on the driver side window and the acoustic field is indirectly determined in order to obtain the right noise level inside the car. Unfortunately in the side-window region

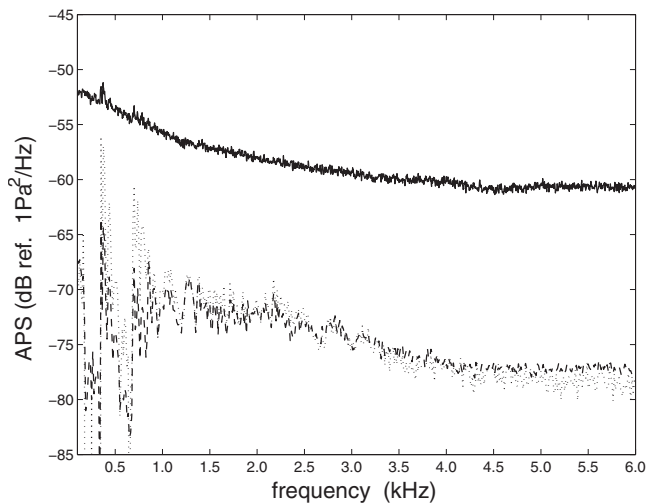


FIG. 12. Measured auto-power spectral (APS) density in solid line. Acoustic part estimated by integration of $\Phi(\vec{k}, \omega)$ over the acoustic disk in dashed line, and acoustic part estimated by Corcos-like model (12) in dotted line.

where the turbulent pressure field is measured, the flow is massively separated, with A-pillar vortex and side mirror wake. The indirect estimation of the acoustic level is also very sensitive to the approximation made in the SEA models used for the window and the passenger compartment. Consequently, a direct comparison with the present results should be made with caution.

The rather high acoustic magnitude found in the present study may be explained by the confined configuration of the turbulent boundary layer since the wind tunnel was especially constructed to minimize acoustic contamination by blower and ambient noise. Moreover the importance of the acoustic contribution induced by wall turbulent flows remains largely unclear. Numerical simulations should complement measurements of boundary layer noise in future investigations, as recently shown by Hu, Morfey and Sandham³³ for the case of an incompressible turbulent channel flow at moderate Reynolds numbers up to $Re^* = u^*h/\nu \leq 1440$. Lighthill's analogy is applied using direct numerical simulation data to estimate the radiated acoustic pressure field, and the dipolar contribution of the wall shear stress varying as $(u^*/c_\infty)^3$ is found to be the dominant contribution at low Mach number and at low frequencies relative to the classical quadrupole radiation in their configurations. By comparison, the Reynolds number in the present work is $Re^* \approx 2.7 \times 10^4$, but the considered frequency $f^+ = f\nu/u^{*2} \approx 5.9 \times 10^{-3}$ is representative of the possible dipolar contribution.³³

Even if the confined configuration of the flow can induce an over-estimation of the acoustic level compared to a free-field boundary layer, this experimental study shows that the acoustic pressure generated by this simple wall flow represents few percents, around 5%, of total pressure field. As the difference of the transmission efficiencies of a glass panel submitted to an acoustic or an aerodynamic pressure field can reach 30 dB, acoustic components of aeroacoustic excitation must be taken into account for interior noise models in automotive industry. The direct measurement of these acous-

tic components in industrial configurations remains an open problem but first attempts have been made using the experimental arrangement presented in this work.³⁴

V. CONCLUSIONS

Direct measurements of the wavenumber-frequency spectrum of wall pressure fluctuations beneath a turbulent boundary layer have been performed using an original rotative array of 63 remote microphone probes. A grid of $63 \times 63 = 3969$ measuring points has then been built up. An original post-processing has been developed to separate the acoustic and the aerodynamic components. The acoustic part has also been estimated from a simple Corcos-like model including the contribution of a diffuse sound field, and these two approaches are found in good agreement. The measured noise contribution is about 5% of the aerodynamic amplitude in the present turbulent channel flow. It should be observed that the broadband acoustic component can only be detected if the aerodynamic level in the low wavenumber region is not too high, which is the case for low Mach number flows. Finally, this value is found rather high with respect to semi-empirical models currently used in automobile applications, and is of importance to predict interior wind noise. The direct acoustic contribution represents only a small fraction of the wall pressure loading but this component is also more easily transmitted to the passenger compartment. It seems thus necessary to take both contributions into account to estimate car interior noise.

ACKNOWLEDGMENTS

The authors would like to thank Pascal Souchotte and Pierre Roland for their technical assistance in the measurements. This work was supported by Renault. C.B. is also with Institut Universitaire de France.

NOMENCLATURE

- c_0 = sound speed in the fluid (air)
- k_c = convective wavenumber, $k_c = \omega / U_c$
- k_f = free flexural wavenumber, $k_f^4 = \rho_s \omega^2 / D$ for an infinite plate of rigidity D and surface density ρ_s
- k_0 = acoustic wavenumber, $k_0 = \omega / c_0$
- u^* = friction velocity
- U_c = convection velocity
- $S_{p_i p_j}$ = cross-power spectral density between points \vec{x}_i and \vec{x}_j (Pa^2/Hz)
- Φ = wavenumber-frequency power spectral density ($\text{Pa}^2 \text{ m}^2 \text{ s}/\text{rad}^3$)
- ω = angular frequency, $\omega = 2\pi f$

¹W. E. Blake, *Mechanics of Flow-Induced Sound and Vibration. II. Complex Flow-Structure Interactions* (Academic, Orlando, FL, 1986), pp. 497–594.

²W. K. Bull, “Wall-pressure fluctuations beneath turbulent boundary layers: Some reflections on forty years of research,” *J. Sound Vib.* **190**, 299–315 (1996).

³W. R. Graham, “A comparison of models for the wavenumber-frequency

spectrum of turbulent boundary layer pressures,” *J. Sound Vib.* **206**, 541–565 (1997).

⁴A. R. George, J. F. Carr and J. R. Callister, “Recent advances in understanding automobile aerodynamic noise,” Paper No. CEAS/AIAA-95-004.

⁵P. G. Bremner and J. F. Wilby, “Aero-vibro-acoustics: Problem statement and methods for simulation-based design solution,” AIAA Paper No. 2002-2551.

⁶R. G. DeJong, T. S. Bharj and J. J. Lee, “Vehicle wind noise analysis using a SEA model with measured source levels,” SAE Paper No. 2001-01-1629.

⁷C. Caccioliati, P. Neple, E. Guyader, J. L. Guyader, and N. Totaro, “Comparison of the vibroacoustic behaviour of a rectangular thin plate excited by a diffuse sound field and a turbulent boundary layer,” in Proceedings of ICSV 13, (2006).

⁸P. Ibars, “Contribution des petits nombres d’onde au champ pariétal de pression dans une couche limite turbulente bidimensionnelle. Comparaison de différentes techniques expérimentales (Small wavenumber contribution to the wall pressure in a turbulent boundary layer. Comparison between different techniques),” Ph.D. thesis, Ecole Centrale de Lyon, Ecully Cedex, France (1990).

⁹E. Manoha, “Mesure du spectre en fréquences et nombres d’ondes du champ des fluctuations de pression pariétale sous une couche limite turbulente (Wavenumber-frequency spectrum measurements of wall pressure fluctuations beneath a turbulent boundary layer),” Ph.D. thesis, Université Paris, Paris, France (1993).

¹⁰B. M. Abraham and W. L. Keith, “Direct measurements of turbulent boundary layer wall pressure wavenumber-frequency spectra,” *J. Fluids Eng.* **120**, 29–39 (1998).

¹¹G. Robert, “Modélisation et simulation du champ exciteur induit sur une structure par une couche limite turbulente (Modelling and simulation of the wall field induced by a structure beneath a turbulent boundary layer),” Ph.D. thesis, Ecole Centrale de Lyon, Ecully Cedex, France (1984).

¹²G. Maidanik, “Flush-mounted pressure transducer systems as spatial and spectral filters,” *J. Acoust. Soc. Am.* **42**, 1017–1024 (1967).

¹³G. Maidanik and D. W. Jorgensen, “Boundary wave-vector filters for the study of the pressure field in a turbulent boundary layer,” *J. Acoust. Soc. Am.* **42**, 494–501 (1967).

¹⁴P. Bally, P. Olivero, P. Hocquet, and B. E. Forestier, “Spectre nombre d’onde-fréquence des fluctuations de pression sous couche limite turbulente en gradient de pression nul et positif (Wavenumber-frequency spectrum of pressure fluctuations beneath a positive pressure-gradient turbulent boundary layer),” *J. Acoust.* **3**, 125–136 (1990).

¹⁵W. K. Blake and D. M. Chase, “Wavenumber-frequency spectra of turbulent boundary-layer pressure measured by microphone arrays,” *J. Acoust. Soc. Am.* **49**, 862–877 (1971).

¹⁶G. M. Corcos, “Resolution of pressure in turbulence,” *J. Acoust. Soc. Am.* **35**, 192–199 (1963).

¹⁷C. H. Sherman, S. H. Ko, and B. G. Buehler, “Measurement of the turbulent boundary layer wave-vector spectrum,” *J. Acoust. Soc. Am.* **88**, 386–390 (1990).

¹⁸R. M. Lueptow, “Transducer resolution and the turbulent wall pressure spectrum,” *J. Acoust. Soc. Am.* **97**, 370–378 (1995).

¹⁹J. R. Callister, “Measurement, prediction, and reduction of the transmission of separated flow noise through panels,” Ph.D. thesis, Faculty of the Graduate School of Cornell University, Ithaca, NY (1996).

²⁰T. M. Farabee and M. J. Casarella, “Measurement of fluctuating wall pressure for separated/reattached boundary layer flows,” *ASME J. Vib., Acoust., Stress, Reliab. Des.* **108**, 301–307 (1986).

²¹T. M. Farabee and M. J. Casarella, “Spectral features of wall pressure fluctuations beneath turbulent boundary layers,” *Phys. Fluids A* **3**, 2410–2420 (1991).

²²T. A. Brungart, G. C. Lauchle, S. Deutschland, and E. T. Riggs, “Wall pressure fluctuations induced by separated/reattached channel flow,” *J. Sound Vib.* **251**, 558–577 (2002).

²³B. Arguillat, “Etude expérimentale et numérique de champs de pression pariétale dans l’espace des nombres d’onde, avec application aux vitrages automobiles (Experimental and numerical study of wall pressure fields in wavenumber-frequency space, with application to automotive glass),” Ph.D. thesis, Ecole Centrale de Lyon, Ecully Cedex, France (2006).

²⁴D. J. J. Leclercq and X. Bohineust, “Investigation and modelling of the wall pressure field beneath a turbulent boundary layer at low and medium frequencies,” *J. Sound Vib.* **257**, 477–501 (2002).

²⁵M. Sunyach, B. Brunel, and G. Comte-Bellot, “Performances de la

- soufflerie anéchoïque à grandes vitesses de l'École centrale de Lyon (Qualifications of the anechoic high-speed wind tunnel of Ecole Centrale de Lyon)," *Rev. Acoust.* **73**, 316–330 (1985).
- ²⁶R. L. Panton and G. Robert, "The wavenumber-phase velocity representation for the turbulent wall-pressure spectrum," *J. Fluids Eng.* **116**, 477–483 (1994).
- ²⁷W. E. Blake, *Mechanics of Flow-Induced Sound and Vibration. I. General Concepts and Elementary Sources* (Academic, Orlando, FL, 1986), pp. 11–30.
- ²⁸B. K. Blake and R. V. Waterhouse, "The use of cross-spectral density measurements in partially reverberant sound fields," *J. Sound Vib.* **54**, 589–599 (1977).
- ²⁹H. Nélisse and J. Nicolas, "Characterization of a diffuse field in a reverberant room," *J. Acoust. Soc. Am.* **101**, 3517–3524 (1997).
- ³⁰J. A. Cockburn and J. E. Robertson, "Vibration response of spacecraft shrouds to in-flight fluctuating pressures," *J. Sound Vib.* **33**, 399–425 (1974).
- ³¹B. M. Efimtsov, "Characteristics of the field of turbulent wall pressure fluctuations at large Reynolds numbers," *Sov. Phys. Acoust.* **28**, 289–292 (1982).
- ³²A. V. Smol'yakov and V. M. Tkachenko, "Model of a field of pseudosonic turbulent wall pressures and experimental data," *Sov. Phys. Acoust.* **37**, 627–631 (1991).
- ³³Z. W. Hu, C. L. Morfey, and N. D. Sandham, "Sound radiation from a turbulent boundary layer," *Phys. Fluids* **18**, 098101 (2006).
- ³⁴H. Illy and D. Ricot, "Étude de la structure de l'excitation aéroacoustique de vitrages automobiles (Characterization of the aeroacoustic excitation of automotive glass)," in *19th Congrès Français de Mécanique* (2009).